Journal of Applied Remote Sensing

RemoteSensing.SPIEDigitalLibrary.org

New geo-portal for MODIS/SEVIRI image products with geolocation-based retrieval functionality

Jorge Sevilla
Yves Julien
Guillem Sória
José A. Sobrino
Antonio Plaza

SPIE.

New geo-portal for MODIS/SEVIRI image products with geolocation-based retrieval functionality

Jorge Sevilla,[a,*] Yves Julien,[b] Guillem Sória,[b] José A. Sobrino,[b] and Antonio Plaza[a]

[a]University of Extremadura, Department of Technology of Computers and Communications, Escuela Politécnica, Hyperspectral Computing Laboratory, Avda. de la Universidad s/n, Cáceres 10003, Spain

[b]University of Valencia, Global Change Unit, Imaging Processing Laboratory, C/ Catedrático Agustín Escardino No. 9, Paterna 46980, Spain

Abstract. A large number of remote sensing data sets have been collected in recent years by Earth observation instruments such as the moderate resolution imaging spectroradiometer (MODIS) aboard the Terra/Aqua satellite and the spinning enhanced visible and infrared imager (SEVIRI) aboard the geostationary platform Meteosat Second Generation. The advanced remote sensing products resulting from the analysis of these data are useful in a wide variety of applications but require significant resources in terms of storage, retrieval, and analysis. Despite the wide availability of these MODIS/SEVIRI products, the data coming from these instruments are spread among different locations and retrieved from different sources, and there is no common data repository from which the data or the associated products can be retrieved. We take a first step toward the development of a geo-portal for storing and efficiently retrieving MODIS/SEVIRI remote sensing products. The products are obtained using an automatic system that processes the data as soon as they are provided by the collecting antennas, and then the final products are uploaded with a one day delay in the geo-portal. Our focus in this work is on describing the design and efficient implementation of the geo-portal, which allows for a user-friendly and effective access to a full repository of MODIS/SEVIRI advanced products (comprising tens of terabytes of data) using geolocation retrieval capabilities. The geo-portal has been implemented as a web application composed of different layers. Its modular design provides quality of service and scalability (capacity for growth without any quality losing), allowing for the addition of components without the need to modify the entire system. On the client layer, an intuitive web browser interface provides users with remote access to the system. On the server layer, the system provides advanced data management and storage capabilities. On the storage layer, the system provides a secure massive storage service. An experimental evaluation of the geo-portal in terms of efficiency and product retrieval accuracy is also presented and discussed.
 [DOI: 10.1117/1.JRS.9.096079]

Keywords: MODIS; SEVIRI; geo-portal; digital repository; geolocation-based image retrieval; remote sensing products; share; web.

Paper 14690 received Nov. 14, 2014; accepted for publication Jan. 27, 2015; published online Feb. 24, 2015.

1 Introduction

In the last years, a significant amount of data from satellite Earth observation instruments has been made available to the public. Among these, the moderate resolution imaging spectroradiometer (MODIS) and the spinning enhanced visible and infra-red imager (SEVIRI) sensors improve on their predecessors. MODIS is a key instrument aboard the Terra/Aqua satellite.[1–4] Terra's orbit around the Earth is timed so that it passes from north to south across the equator around 10:30, while Aqua passes south to north over the equator around 13.30. Global coverage

*Address all correspondence to: Jorge Sevilla, E-mail: jorgesece@unex.es

1931-3195/2015/$25.00 © 2015 SPIE

of the Earth is provided by Terra/Aqua every 1 to 2 days. On the other hand, the SEVIRI instrument on board the geostationary platform Meteosat Second Generation (MSG)[5] provides (every 15 min) a low resolution scan of Europe, Africa, the Middle East, and the eastern tip of South America. The images have a sub-nadir resolution of 3 km that deteriorates toward the poles, reducing to an average of 5×3 km^2 over Europe.

In recent years, many research studies have focused on the calibration and exploitation of data coming from the aforementioned instruments.[5–8] For instance, in Ref. 9, an operational algorithm for retrieving the land surface temperature (LST) from SEVIRI data is provided. In Ref. 10, a technique for estimating the sea surface temperature (SST) from SEVIRI data is given. A similar strategy is developed in Refs. 11 and 12 for MODIS data, while Ref. 13 assessed the presence of trends in the MODIS time series. In Ref. 14, a procedure for water vapor retrieval from SEVIRI observations is presented. Numerous classic studies,[15,16] have also focused on the retrieval of advanced vegetation parameters from remote sensing data such as normalized difference vegetation index (NDVI) or fraction of vegetation cover (FVC), with the ultimate goal of providing advanced products covering relatively large areas.[17] Several other recent applications have exploited MODIS data in a diversity of areas, such as estimation of vegetation phenology,[18] mapping of snow cover,[19] characterization of soil moisture,[20] mapping of impervious cover,[21] agriculture monitoring,[22] analysis of LST and environmental factors,[23] deriving water fraction and flood maps,[24] or fire characterization,[25] among many others.[26–28] SEVIRI data have also been recently exploited for phenology estimation,[29] detection of tropical cyclones,[30] monitoring aerosols,[31] or estimating land surface radiation and energy budgets from ground measurements.[32] These studies are possible thanks to the availability of a wide range of advanced remote sensing products from the data collected by those instruments.

There are several institutions currently distributing multispectral sensors products. On one hand, the NASA Earth observing system data and information system (EOSDIS) provides end-to-end capabilities for managing NASA's Earth science data from various sources (satellites, aircraft, field measurements, and various other programs) in which the data are distributed through the LAADS Web[33] system. This system provides quick and easy access to MODIS Level 1, atmosphere and land data products and visible infrared imaging radiometer suit sensor Level 1, and land data products. On the other hand, the land processes distributed active archive center from USGS distributes mainly land products through several web systems, of which two of them are focused on MODIS products. First, the USGS EE[34] tool offers data from the Landsat missions and a variety of other data providers. This tool now provides access to MODIS land data products (from the NASA Terra and Aqua missions) and to ASTER level-1B data products over the U.S. territories (from the NASA ASTER mission). The second web system of USGS is MRTWeb 2.0,[35] which is a more complete data system that combines the interface of USGS global visualization viewer[36] and the product database of MRT.[37] In our work, we propose an alternative repository that combines products from two very different resolution sensors: MODIS and SEVIRI, which provide images and products with different formats.

The calibration of Earth observation satellites in the Spain (CEOS-SPAIN) project has recently developed a fullly operational chain for advanced retrieval and processing of MODIS and SEVIRI data acquired in real time at the global change unit (UCG), image processing laboratory (IPL),[38] University of Valencia (see Fig. 1). These final products are validated (quality control) using the on-ground data acquired in a variety of test sites. The UCG/IPL participated actively in the definition of products to be delivered to users from MODIS and SEVIRI data. The resulting remote sensing products are of great interest for the wide remote sensing community. These MODIS products cover Southwestern Europe and most of Northwestern Africa, while SEVIRI products cover half the surface of the Earth. However, the wide availability of these products is difficult due to the massive volume of information that they comprise. In the case of MODIS, the amount of data acquired and processed by UCG/IPL from July 2010 to October 2014 exceeds 9000 images and 200,000 resulting products (more than 11 terabytes of products). In the case of SEVIRI, the amount of data acquired and processed by UCG/IPL from July 2007 to October 2014 comprises more than 300,000 images and 600,000 resulting products (more than 17 terabytes of products). This massive amount of information can be extremely useful in climate change studies and in many other studies, especially if the products could be easily retrieved for a given area of interest. In fact, this capability has the potential to impact the

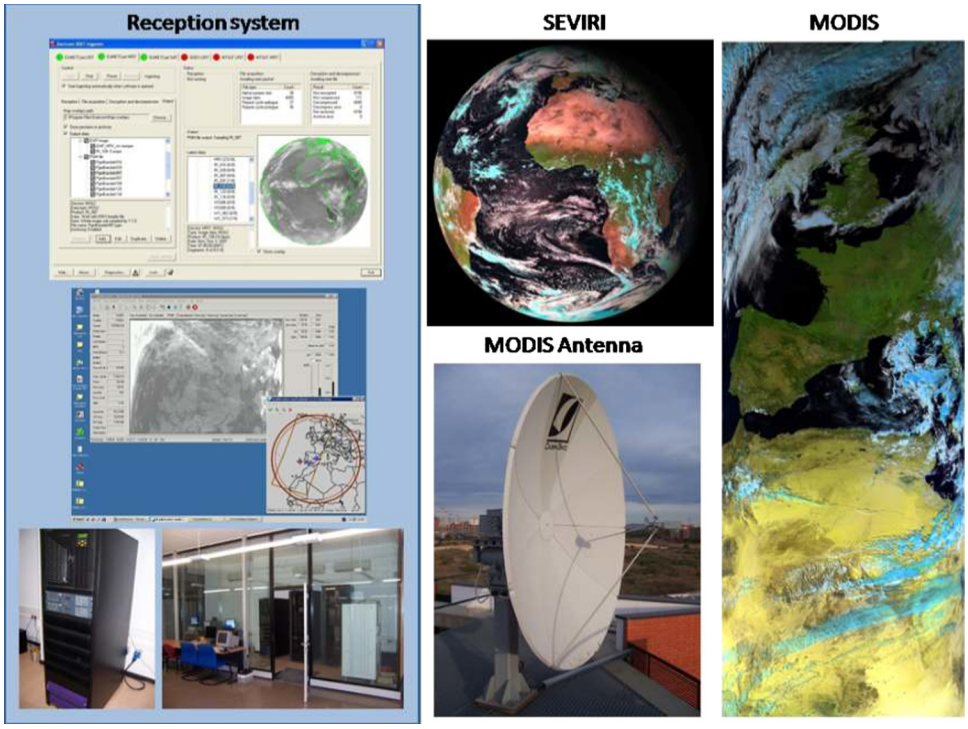

Fig. 1 MODIS (Terra/Aqua) and SEVIRI (Meteosat Second Generation) real-time reception system at the Global Change Unit (UCG) within the Image Processing Laboratory (IPL) of the University of Valencia.

activities of many remote sensing users such as farmers, engineers and water managers, as well as the scientific community.

In this paper, we describe a new geo-portal that has been specifically designed to provide efficient access to a large collection of the products of MODIS/SEVIRI image acquisitions, which are generated in near real time at the facilities of UCG/IPL. This work is the first to be published on the reception system at IPL. The geo-portal has been designed in the framework of the CEOS-SPAIN project, which ultimately pursues the development of an integrated system for optical data validation and information extraction, and is expected to serve as a reference to the remote sensing community through the heterogeneous data distribution and dissemination mechanisms planned for the project. The geo-portal has been designed using an advanced computing infrastructure to speed up the supported data distribution and processing tasks. The geo-portal works as a digital repository which has been designed in order to store and efficiently retrieve advanced MODIS/SEVIRI products. Of particular importance are the geolocation-based retrieval functionalities included in the geo-portal, which facilitates searching for remotely sensed scenes (in geolocated form) over a map using Google Maps services.[39] Although the geo-portal is focused on Southwestern Europe, it is designed to store images from any location. Another feature of our geo-portal is that it provides advanced products which may be useful to end-users without the capability to perform advanced processing of the collected remote sensing data. In fact, the idea of using the final products instead of the raw data is quite appealing from the viewpoint of the end-user, who can simply retrieve the processed products after applying different types of indices and perform a more intuitive exploitation of the data.

The proposed geo-portal has been implemented as a web application[40] and is composed of different layers. Its modular design provides quality of service and scalability, and allows adding and/or modifying components without the need to modify the entire system. These properties result from the fact that the geo-portal has been developed as a digital repository using advanced software and hardware design techniques with the most advanced tools for such purposes currently available. On the client layer, an intuitive web browser interface provides users with remote access to the system. On the server layer, the system provides advanced data management capabilities. On the storage layer, the system provides a safe massive storage service handling

several terabytes of data. Combined, these parts provide a completely open standardized repository of (easily searchable) MODIS/SEVIRI products that is expected to be useful in a variety of remote sensing data exploitation tasks, as originally intended by the CEOS-SPAIN initiative.

The remainder of this work is organized as follows. Section 2 describes the processing chain used to generate the advanced MODIS/SEVIRI products that are distributed through the geo-portal. This chain is applied as soon as the data are collected, and the system automatically stores the resulting products in the geo-portal. Section 3 describes the implementation of the geo-portal which is composed of three main layers: (1) client layer, which defines the interaction between the user and the system through a web interface; (2) server layer, which efficiently manages the requests coming from end-users; and (3) storage layer, in charge of safe storage and retrieval of remote sensing products. Section 4 presents an experimental validation of the system, with particular attention to its geolocation retrieval accuracy and to the performance of the system in responding to the queries carried out by end-users. Section 5 concludes the paper with some remarks and hints at plausible future research lines.

2 Processing Chain

We have implemented a processing chain for MODIS (Terra/Aqua) and SEVIRI (MSG) data acquired in real time with the antennas located at the UCG/IPL of the University of Valencia. SEVIRI data encompass the hemisphere centered on the (0,0) latitude/longitude coordinates, while acquired MODIS data consist of Aqua and Terra overpasses within the reach of the antenna located at the IPL, which mostly covers Western Europe and Maghreb. These data allow for the generation of classic and advanced remote sensing products for inter-comparison with other sensor products. The proposed chain has been designed for processing image acquisitions every day, and is applied in near real time (i.e., soon after the data are collected). The chain is implemented in the interactive data language (IDL).[41] This section succintly describes the process carried out over MODIS (Sec. 2.2), and then SEVIRI (Sec. 2.3) data. Both cases need a previous preprocessing step which is described in Sec. 2.1.

2.1 *Preprocessing*

For both MODIS and SEVIRI sensors, images are acquired as digital counts, which are converted to radiances using the gain and offset values provided in the metadata associated with the images. Then the day-time visible and near infra-red (NIR) channels of the data are atmospherically corrected using a simplified method for the atmospheric correction (SMAC) of satellite measurements in the solar spectrum.[42] The choice of standard input values for atmospheric correction with SMAC software results in a compromise between atmospheric correction accuracy and instantaneous processing of the received data. By using standard values, the atmospheric corrected values for atmosphere type (continental), atmospheric pressure (1013 hPa), aerosol optical thickness (0.05), and ozone concentration (0.33 atm.cm), may be slightly over- or under-estimated, although the resulting error is generally lower than the error resulting from the use of the top of the atmosphere values. This method runs on a pixel-by-pixel basis, and needs additional information such as (standard values in parentheses): atmosphere type (continental), atmospheric pressure (1013 hPa), aerosol optical thickness (0.05), and ozone concentration (0.33 atm.cm). Additionally, a water vapor product (see below) is needed as an input for the SMAC software. Finally, for thermal infra-red channels, brightness temperatures are estimated by inverting Planck's law:

$$\mathbf{T}_i = \frac{\frac{\mathbf{c}_2}{\lambda_{\text{eff}}}}{\ln\left[\frac{\mathbf{c}_1}{\lambda_{\text{eff}}^5 \cdot \mathbf{B}(\mathbf{T}_i)} + 1\right]}, \tag{1}$$

where $\mathbf{T}_i$ is the brightness temperature in each thermal band, $\mathbf{c}_1 = 1.1491047 \cdot 10^8$ W/$(\text{m}^2\,\text{sr}\mu\text{m}^{-4})$, $\mathbf{c}_2 = 1.4387752 \cdot 10^4$ K $\cdot\, \mu$m, $\mathbf{B}(\mathbf{T}_i)$ is the at sensor radiance, expressed in W/$(\text{m}^2\,\text{sr}\mu\text{m})$, and λ_{eff} is the effective wavelength for each band i.

2.2 *MODIS Products*

The complete set of products available in our system is described hereafter. Ancillary data include latitude, longitude, elevation (height), sensor azimuth angle, sensor zenith angle, solar azimuth angle, and solar zenith angle. Several masks can also be downloaded: land/sea mask, day/night mask (day), cloud mask (clouds), fire mask (fire), and snow mask (snow). These masks have been calculated with MOD35 and MOD14 software.[43] Advanced products, including vegetation condition index[44] and bidirectional reflectance distribution function (BRDF)[45] corrected NDVI and reflectances for bands 1 to 7, will be included in the near future. Additionally, other products are available in our system:

- NDVI[15] is traditionally calculated as $\mathrm{NDVI} = (\mathrm{NIR} - \mathrm{RED})/(\mathrm{NIR} + \mathrm{RED})$, where NIR stands for reflectivity in NIR, and RED stands for reflectivity in red channels, which for MODIS correspond, respectively, to MODIS bands 2 and 1

$$\mathrm{NDVI} = \frac{\rho_2 - \rho_1}{\rho_2 + \rho_1}, \tag{2}$$

  where ρ_1 and ρ_2 are the at-surface reflectivities obtained from sensor bands located in RED and NIR spectral regions.
- FVC is estimated from the NDVI following Ref. 16 for day-time acquisitions, as a normalization of the NDVI between standard bare soil and dense vegetation values. In the case of MODIS, these values are 0.15 and 0.90, respectively[17]

$$\mathrm{FVC} = \frac{\mathrm{NDVI} - 0.15}{0.90 - 0.15}. \tag{3}$$

- Emissivities are estimated for day-time acquisitions from FVC and MODIS band 1 information, following the methodology presented in Ref. 12. These emissivities correspond to MODIS thermal bands 31 and 32, and are estimated differently depending on the vegetation proportion within a given pixel. In the case of night-time acquisitions, such a method cannot be implemented due to the lack of solar radiation; therefore, the emissivity estimates during the previous day are re-projected to a latitude/longitude grid, averaged, and re-projected back to the night-time acquisition configuration for further calculations. Due to computational constraints, the re-projection algorithm is limited to the Iberian Peninsula and North West Africa. Therefore, night products are also limited to this area. As Table 1 shows, the emissivities are expressed as average emissivities ε (for bands 31 and 32) and spectral difference of emissivities $\mathbf{\Delta}\varepsilon$.
- Water vapor is then estimated using the method developed in Ref. 12. This method is based on the attenuation of surface reflected solar radiation and clouds in NIR due to water vapor. To this end, water vapor absorbing bands centered at 0.905, 0.936 and 0.94 μm (bands 17, 18 and 19) are used in addition to a water vapor transparent band centered at 0.865 μm (band 2) as follows:

$$\mathbf{W} = 0.192 \cdot \mathbf{W}_{17} + 0.453 \cdot \mathbf{W}_{18} + 0.355 \cdot \mathbf{W}_{19}, \tag{4}$$

  where

Table 1 Moderate resolution imaging spectroradiometer (MODIS) emissivity values.

	ε	$\Delta\varepsilon$
Vegetation: NDVI > 0.5	0.99	0
Mixed: $0.2 \leq \mathrm{NDVI} \leq 0.5$	$0.971 + 0.018\mathrm{FVC}$	$0.006(1 - \mathrm{FVC})$
Bare soil: NDVI < 0.2	$0.9832 - 0.058\rho_1$	$0.0018 - 0.060\rho_1$

$$\mathbf{W}_{17} = 28.449 \cdot \mathbf{G}_{17}^2 - 54.434 \cdot \mathbf{G}_{17} + 26.314,$$
$$\mathbf{W}_{18} = 27.884 \cdot \mathbf{G}_{18}^2 - 23.017 \cdot \mathbf{G}_{18} + 5.012,$$
$$\mathbf{W}_{19} = 19.914 \cdot \mathbf{G}_{19}^2 - 26.887 \cdot \mathbf{G}_{19} + 9.446,$$

with

$$\mathbf{G}_{17} = \mathbf{L}_{17}/\mathbf{L}_2,$$
$$\mathbf{G}_{18} = \mathbf{L}_{18}/\mathbf{L}_2,$$
$$\mathbf{G}_{19} = \mathbf{L}_{19}/\mathbf{L}_2,$$

where $\mathbf{W}$ is the atmospheric water vapor ($g \cdot cm^{-1}$), and $\mathbf{L}_2$, $\mathbf{L}_{17}$, $\mathbf{L}_{18}$ and $\mathbf{L}_{19}$ are the radiance values (RAD-TOA) of MODIS in 2, 17, 18, and 19 bands, respectively. In the case of night-time acquisitions, such a method cannot be implemented due to the lack of solar radiation; therefore, the water vapor estimates during the previous day are re-projected to a latitude/longitude grid, averaged, and re-projected back to the night-time acquisition configuration for further calculations. Even though different water vapor values are estimated for any given day, only one water vapor value (daylight average of valid values) is considered per day. Assuming a constant water vapor during 24 h may lead to over- and under-estimations of this parameter, resulting in small differences in final LST. A sensibility analysis shows that an error of $1 g \cdot cm^2$ in water vapor leads to a 0.23 K error in LST.

- LST is estimated for day- and night-time acquisitions using the method developed in Ref. 12:

$$\mathrm{LST} = \mathbf{T}_{31} + \mathbf{a}_1 + \mathbf{a}_2(\mathbf{T}_{31} - \mathbf{T}_{32}) + \mathbf{a}_3(\mathbf{T}_{31} - \mathbf{T}_{32}) + (\mathbf{a}_4 + \mathbf{a}_5 \cdot \mathbf{W})(1 - \varepsilon) + (\mathbf{a}_6 + \mathbf{a}_7 \cdot \mathbf{W})\delta\varepsilon, \quad (5)$$

where $\mathbf{T}_{31}$ and $\mathbf{T}_{32}$ are the brightness temperatures for MODIS bands 31 and 32, respectively, ε and $\delta\varepsilon$ are respectively the average emissivity and the spectral emissivity difference for these bands, and W is the total amount of water vapor estimated above, and $\mathbf{a}_1 = 1.02$, $\mathbf{a}_2 = 1.79$, $\mathbf{a}_3 = 1.20$, $\mathbf{a}_4 = 34.83$, $\mathbf{a}_5 = -0.68$, $\mathbf{a}_6 = -73.27$ and $\mathbf{a}_7 = -5.19$.

- SST[46] is estimated for day- and night-time acquisitions using

$$\mathrm{SST} = \mathbf{T}_{31} + (\mathbf{a}_1 + \mathbf{a}_2 \cdot \mathbf{W})(\mathbf{T}_{31} - \mathbf{T}_{32}) + \mathbf{a}_3 \cdot \mathbf{W} + \mathbf{a}_4, \quad (6)$$

where $\mathbf{T}_{31}$ and $\mathbf{T}_{32}$ are the brightness temperatures for MODIS bands 31 and 32, respectively, $\mathbf{W}$ is the total amount of water vapor estimated above, and $\mathbf{a}_1 = 1.90$, $\mathbf{a}_2 = 0.44$, $\mathbf{a}_3 = 0.05$ and $\mathbf{a}_4 = 0.34$.

2.3 *SEVIRI Products*

The SEVIRI products available in our processing chain can be summarized as follows:

- NDVI is retrieved as in the case of MODIS data, by using red (visible band at 0.6 μm) and NIR (visible band 0.8 μm) information.
- Emissivities are estimated for day-time acquisitions from NDVI and red information at 0.6 μm (Vis06), following the threshold method. These emissivities correspond to SEVIRI infrared $\mathbf{T}_{108}$ and $\mathbf{T}_{120}$ spectral bands centred at 10.8, and 12.0 μm, and are estimated differently depending on the vegetation proportion (PV) within a given pixel. These emissivities are expressed as ε_{108} and ε_{120}. However, as Table 2 shows, the coefficients for emissivity estimation for different NDVI ranges of value where

$$\mathrm{FVC}_{\mathrm{seviri}} = \frac{(\mathrm{NDVI} - 0.2)^2}{0.009}.$$

- Water vapor is then estimated using the method developed by Ref. 12. This method is based on the difference in temperature between two different acquisitions ($\mathbf{T}^A$ and $\mathbf{T}^B$) for both infra-red channels ($\mathbf{T}_{108}$ and $\mathbf{T}_{120}$) centered at 10.8 and 12.0 μm, and depends

Table 2 Spinning enhanced visible and infrared imager (SEVIRI) emissivity values.

	ε_{108}	ε_{120}
Vegetation: NDVI > 0.5	0.99	0.99
Mixed: 0.2 ≤ NDVI ≤ 0.5	$0.968 + 0.021\text{FVC}_{\text{seviri}}$	$0.976 + 0.015\text{FVC}_{\text{seviri}}$
Bare soil: NDVI < 0.2	0.977 – 0.048Vis06	0.981 – 0.026Vis06

on the observation zenith angle (θ). This temperature difference should be greater than 10 K for the method to be accurate

$$\mathbf{W} = \mathbf{a} \cdot \arg^2 + \mathbf{b} \cdot \beta + \mathbf{c}, \tag{7}$$

where $\mathbf{a} = -15.1 \cdot \sec\theta + 5.1$, $\mathbf{b} = 16.4 \cdot \sec\theta - 2.8$, $\mathbf{c} = 0.336 \cdot \sec\theta - 0.117$, and

$$\beta = \frac{1}{\sec\theta} \ln\left(\frac{\mathbf{T}_{108}^{A} - \mathbf{T}_{108}^{B}}{\mathbf{T}_{120}^{A} - \mathbf{T}_{120}^{B}}\right).$$

However, this method provides only a few values per day, which can lead to errors in the case of rapidly evolving weather conditions. To address this issue, methods for instantaneous estimation of water vapor are currently being investigated.[47]

- LST is estimated for day- and night-time acquisitions using the method developed in Ref. 14 as follows:

$$\begin{aligned}\text{LST} = {} & \mathbf{T}_{108} + \left[1.34 - \frac{0.11}{\cos^2\theta}\right] \cdot (\mathbf{T}_{108} - \mathbf{T}_{120}) + \left[0.29 + \frac{0.08}{\cos^2\theta}\right] \cdot (\mathbf{T}_{108} - \mathbf{T}_{120})^2 \\ & + \left[60.67 - \frac{10.01}{\cos^2\theta}\right] \cdot (1 - \varepsilon) + \left[-6.71 + \frac{2.47}{\cos^2\theta}\right] \cdot \mathbf{W} \cdot (1 - \varepsilon) \\ & + \left[-125.91 + \frac{15.09}{\cos^2\theta}\right] \cdot \boldsymbol{\Delta}\varepsilon + \left[19.44 - \frac{4.27}{\cos^2\theta}\right] \cdot \mathbf{W} \cdot \boldsymbol{\Delta}\varepsilon + \left[-0.44 + \frac{0.57}{\cos^2\theta}\right],\end{aligned} \tag{8}$$

where $\mathbf{T}_{108}$ and $\mathbf{T}_{120}$ are brightness temperatures for the infra-red bands centered at 10.8 and 12.0 μm (Ir108 and Ir120) respectively, ε and $\boldsymbol{\Delta}\varepsilon$ are, respectively, the average emissivity and the spectral emissivity difference for these bands, W is the total amount of water vapor estimated above, and θ is the observation zenith angle.

- SST is estimated for day- and night-time acquisitions using the method developed in Ref. 10:

$$\begin{aligned}\text{SST} = {} & \mathbf{T}_{108} + (0.99 \cdot \cos\theta + 0.21) \cdot (\mathbf{T}_{108} - \mathbf{T}_{120}) \\ & + \left(\frac{0.364}{\cos\theta} + 0.15\right) \cdot (\mathbf{T}_{108} - \mathbf{T}_{120}) + \frac{0.327}{\cos\theta} + 0.11,\end{aligned} \tag{9}$$

where $\mathbf{T}_{108}$ and $\mathbf{T}_{120}$ are the brightness temperatures for MSG bands Ir108 and Ir120, respectively.

3 Geo-Portal

This section is devoted to the description of our proposed geo-portal system. In Sec. 3.1, we describe the system architecture of the geo-portal and the different layers that compose it. In Sec. 3.2, we describe the structure of the database that stores the associated metadata of the MODIS/SEVIRI scenes and their products. Section 3.3 describes how the queries to the database are performed in the system. Finally, Sec. 3.4 describes the procedure used by the geo-portal to retrieve and provide advanced remote sensing scenes and their products to end-users.

3.1 *System Architecture*

As shown in Fig. 2, the architecture of the proposed system is composed of different layers which can be defined by their roles. The system follows a modular design in which the communication between layers is performed using standard data exchange formats and transfer protocols, so that any layer can be easily modified and/or enhanced as long as its connectivity with the remaining layers of the system is maintained. More specifically, our design has been carried out using free software tools such as `Symfony2`,[48] a full-stack web framework, while the adopted format for data exchange is JavaScript Object Notation (`JSON`),[49] an open standard format that uses human readable text to transmit data objects. In the following, we describe the different layers that compose the geo-portal.

3.1.1 *Client layer*

This layer defines the interactions between the users (through an internet web browser) and our geo-portal, and is responsible for providing users with remote and interactive access to the system. The web interface has been designed using `HTML5`,[50] which is the most widely used web programming language, and `CSS3`,[51] which is a standard style language for improving the `HTML5` web appearance. In addition, we also used `jQuery`,[52] which is a JavaScript library for controlling the web behavior. The interaction between the user and the web interface is captured by the event handlers of the `jQuery` libraries. The web interface transmits the requests to the server layer via `HTTP`,[53] an application protocol for distributed, collaborative, hypermedia information systems, and the foundation of data communication for the World Wide Web. Most of the views are actually generated in the server using `Symfony2`, a robust web development framework.

3.1.2 *Server layer*

The system is implemented as a web application in the sense that it provides remote access to a set of clients (i.e., the end-users of our system) through Internet connections, so that web pages are delivered to the clients while user requests are received and immediately processed. An advantage of this approach is that no additional software has to be installed on the client node, since

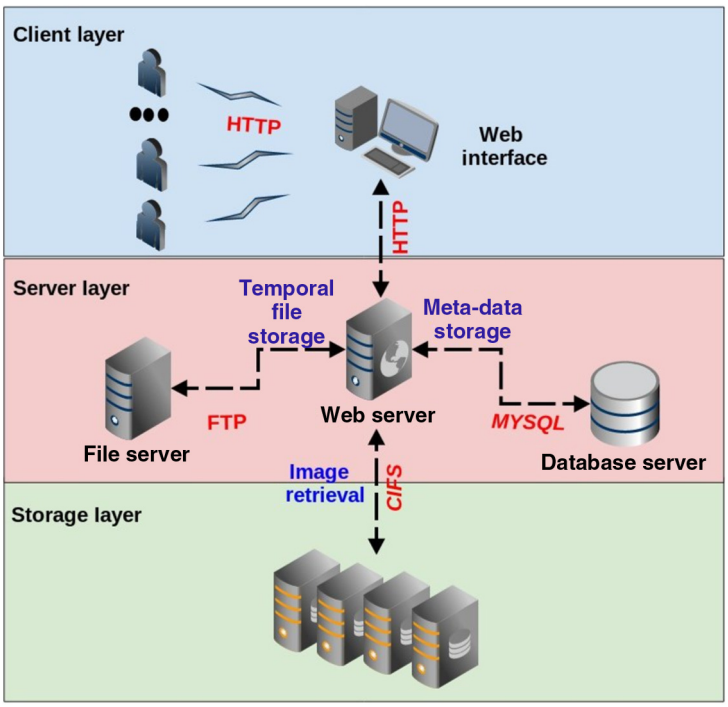

Fig. 2 Architecture of the proposed geo-portal.

only a web browser is required for interacting with the geo-portal. The services provided by the system are managed and executed on the server layer, which is composed of several elements with different roles. As Fig. 2 shows, the web server handles web interface requests (via HTTP) and manages the system resources such as metadata and file data storage. The metadata are associated with the image scene and their products which are used for efficient data retrieval as will be explained in the subsequent sections. The server layer can be considered as the main engine of the system since it is in charge of managing and connecting the different components that integrate it. The server layer is also in charge of storing image and product metadata, following a database scheme that is described in subsection 3.2. For the management of the database we have selected Mysql,[54] an open-source database manager which provides all the necessary requirements for our system, such as stored functions and procedures, fast queries, and low computational cost. This database manager is widely used for building high performance webs. The Mysql database manager allows for the direct efficient execution of stored procedures, which is needed in our context in order to deal with the high computational cost of executing a matching algorithm for data retrieval involving several terabytes of data. On the other hand, we also used an FTP[55] file storage server in this layer for providing remote user access to nonremotely accessible storage layer files. This module is ultimately in charge of providing a temporal file storage of the files related to the user download requests. The files are automatically deleted once a given limit time (parametrized value) is expired. This strategy allows for efficient downloads of the products retrieved by the geo-portal after the end-user queries are completed.

3.1.3 *Storage layer*

The proposed geo-portal has been specifically designed bearing in mind the need to manage and share a large amount of remote sensing data products obtained after applying the MODIS/SEVIRI processing chain described in Sec. 2. The hardware resources utilized in the storage layer comprise a set of DELL NAS[56] processing nodes. First, a DELL PowerVault NX3200[57] system is dedicated to storing the MODIS related products. It consists of a chassis with up to 12 hard SAS[58] drives, and an Intel Xeon E5-2609[59] CPU with 32 GB of RAM memory. Security and high availability is provided by a PERC H710[60] integrated RAID controller which combines multiple hard disks into a logical unit for storage purposes. The overall storage capacity comprises 30 terabytes using RAID 5 and a hot spare unit. On the other hand, a second DELL node is dedicated to storing SEVIRI products. It consists of another DELL PowerVault NX3200 connected to a DELL PowerVault MD1200[61] which provides 24 terabytes of additional storage capacity, for a total of 54 terabytes capacity for the SEVIRI products. Both the PowerVault MD1200 and the PowerVault NX3200 are connected through PERC H800[62] adapters. As mentioned before, the main purpose of this layer is to provide advanced storage capabilities, so all interactions are performed through other layers of the system that directly access this layer. The storage layer and the server layer are located inside a private network which is remotely nonaccessible. Both layers are connected by using the common Internet file system,[63] a protocol that defines a standard for remote file access allowing up to millions of connections at the same time.

3.2 *Database Structure*

Figure 3 illustrates the database scheme used to store remote sensing products in the proposed geo-portal. The database has been designed in order to store information not only from the products, but also from the original remote sensing data (although in our current version only the products are available through the geo-portal). The information stored in the database for each image entry comprises the number of samples, lines, bands, data type, byte order, wavelength information, interleave, thumbnails, geolocation, and sensor used (limited to MODIS/SEVIRI in the present version but fully extensible to other sensor data in future developments). Most importantly, our system also contains information about the presence of cloud areas (called cloudiness hereinafter) in the scene. Clouds were identified through IMAPP[64] Level2 Cloud Mask (MOD35) software. In order to minimize the database size, the geolocation data are confined to the four extreme image coordinates of each data set. In practice, each image is decomposed

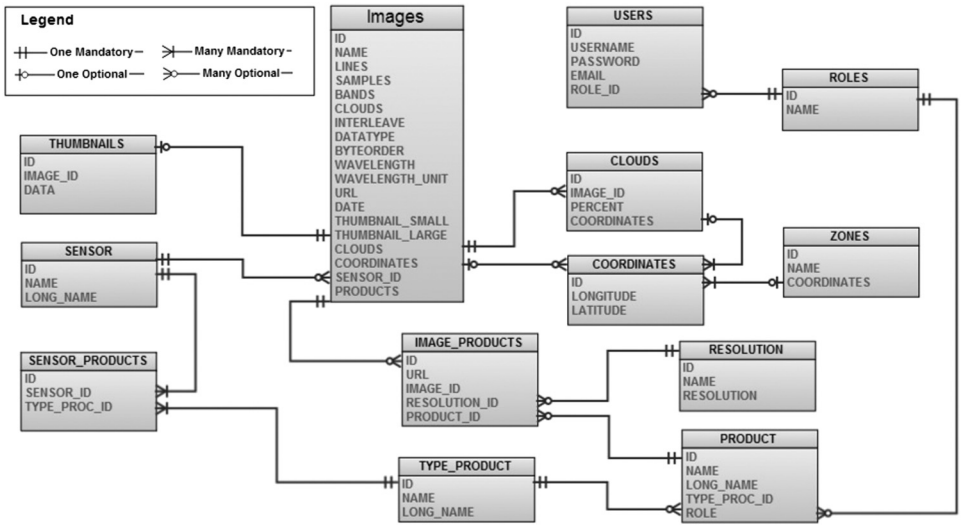

Fig. 3 Structure of the database used to store data and products in the proposed geo-portal.

into 30 parts (called quarters) and we store geolocation and cloudiness information for each quarter. In addition, relevant information about the data products are also stored in the geo-portal, including type of product, resolution, sensor of acquisition, and so on. All this information can be used for retrieval purposes using different queries. At this point, we reiterate that the database structure has been designed to store not only the final products but also the raw data. Although in the current version of the geo-portal, we only make available the final products to external users, the system is also prepared to provide other different data levels (including the raw data). In the following, we describe the database tables design.

3.3 *Queries*

Although the aim of this work is to offer remote sensing products, the retrieval system is designed to retrieve remote sensing scenes which have associated products. Thus, the queries are performed using the image associated metadata, which is the fastest procedure since all the products of an image have the same query parameters.

In this subsection, we outline the queries that can be performed to retrieve remote sensing products in the proposed geo-portal system. The geo-portal includes an advanced retrieval system which provides high query performance. The query filters include acquisition date, used sensor, geolocation, or cloudiness. It should be noted that the last two filters are only available for MODIS images due to the geostationary character of the MSG platform, where geolocation information for the SEVIRI data need not be included within each image. As for cloud information for SEVIRI data, it is still not available, although we plan to include this information in the geo-portal in the near future. In the following, we first describe the searching methodology which relies on a newly developed geolocation matching algorithm. Then we describe the procedure used to perform the search from an end-user's point of view (with particular emphasis on the developed web browser interface and the searching options available in the system). Finally, we describe the procedure used by the system to allow for remote downloads of data from end-users.

3.3.1 *Searching methodology*

In order to deal with the time needed to perform image retrieval on a huge database such as the one available in our geo-portal, the searching functionality has been designed in a way that the queries are completely executed on the database manager engine. This is a very important aspect, since the possibility to perform the queries directly in `Mysql` allows for greatly increased performance as the queries are executed as simple `SQL` calls embedded in the database manager.

In previous versions of the geo-portal, we intended to use an external programming language such as C++ in order to perform the queries, which resulted in a much slower response time. As a result, the embedding of the queries into `Mysql` is considered to be one of the most attractive features of the proposed geo-portal system as this design choice guarantees a high quality of service. The interest region-based searches are implemented by means of a newly developed geolocation matching algorithm, which works as a stored procedure in the database to resolve geolocation-based queries. This algorithm is particularly useful for retrievals based on the MODIS sensor, since this instrument provides images with irregular geolocation that makes it difficult to link the data with a set of given geocoordinates. This introduced significant difficulties since our idea was to visualize and retrieve the obtained products in an interactive fashion based on available map services such as Google Maps. In order to address this issue, we have developed a fast matching algorithm which compares two geographic regions using their four extreme coordinates. This methodology is summarized in Algorithm 1.

As shown by Algorithm 1, the main idea of the proposed geolocation procedure is to establish the overlapping between a user-defined region and the corresponding image region. In other words, the user interactively defines an area of interest over a map service (in our case, by drawing a polygon in Google Maps) and the system should retrieve all the stored products of the images that have some area overlapping with the region defined by the user in an interactive fashion. The matching procedure is described in detail in Algorithm 2. As shown by this algorithm, all comparisons are based on the four extreme coordinates for the user-defined region and for the associated quarters. In order to manage the computational cost of the geolocation procedure, this technique has been designed in the form of an efficient stored procedure implementation, which exploits the high performance of the `Mysql` storage procedure engine and provides low latency in the associated complex queries. At this point, it is important to reiterate that the geographic matching of the regions/quarters is performed using geometric concepts which are based on interpreting the coordinates as points and the regions as planes formed by those points, as described in detail in Algorithm 2. In order to cover all the matching possibilities, we first evaluate whether there is any intersection of lines from both planes and, if this is not the case, we evaluate whether any point from either plane is inside the other plane by using the point-in-polygon approach developed in Ref. 65. As described in Algorithms 1 and 2, the geolocation matching technique executes different queries based on different filter inputs, which can be simply summarized as follows:

- No filters: all the scenes from the same sensor are retrieved.
- Interest region filter: only those scenes in which its geographic region matches with the interest region are retrieved.
- Cloudiness threshold filter: only those scenes in which all quarters contain cloudiness below the threshold are retrieved.
- Cloudiness threshold and interest region filters: only those scenes in which all quarters within the region of interest contain cloudiness below the threshold are retrieved.

3.3.2 *Searching procedure from end-user point of view*

In this subsection, we outline how the searching procedure is conducted from an end-user's point of view. Figure 4 shows the browser interface of the geo-portal, which allows the user to select several filters using a friendly interface. As shown by Fig. 4, the leftmost panel of the browser allows specifying the type of sensor for the retrieval of associated image products, as well as the maximum percentage of clouds allowed in the data to be retrieved. The leftmost panel also allows for the retrieval of image products by date (or range of dates) and by geographic coordinates. On the other hand, as Fig. 4 shows, the main panel of the browser includes a map obtained from Google Maps service. The map panel is fully interactive and allows the user to draw a polygon directly on the map in order to perform the retrieval only in the geographical area delimited by the polygon. In order to achieve this functionality, the geolocation matching technique described in Algorithm 1 and its associated matching procedures, described in Algorithm 2, are used. In the following, we summarize the different steps that a simple query involves:

Algorithm 1 Geolocation matching algorithm.

```
procedure GELOCATIONMATCHING(IMAGES,selectedPoints,maxCloudiness)
    vectorResults = new Vector
    for all IMAGES do
        imagePoints = image.Points
        resultIn = false
        if (No selectedPoints) OR PLANEINTERSECTION(imagePoints, selectedPoints) OR ANYPOINTINPOLYGON
        (imagePoints, selectedPoints) then
            resultIn = true
            if (maxCloudiness) then
                quarters = image.quarters
                for all quarters do
                    quarterPoints = quarter.Points
                    if (PLANEINTERSECTION(quarterPoints, selectedPoints) OR ANYPOINTINPOLYGON(quarterPoints,
                    selectedPoints)) then
                        if quarter.cloudPercent > maxCloudiness then
                            resultIn = false
                            Break For loop
                        end if
                    end if
                end for
            end if
        end if
        if resultIn then
            vectorResults.push(image)
        end if
    end for
    return vectorResults;
end procedure
```

- First, the user can define simple criteria for the query, such as sensor or dates of acquisition, in the leftmost panel of the browser as indicated in Fig. 4.
- In a second step, the user can refine the query by drawing a polygon in the map panel. The geolocation matching technique will be used to retrieve only the images located in a geographic area that has some overlap with the polygon. The system provides other additional options for selecting the region of interest coordinates, such as simple input form or a set of pre-established zones, as indicated in the leftmost panel (see Fig. 4).
- As an optional step, the system allows for defining a maximum cloudiness filter, which is used to restrict images with low visibility due to cloud contamination. After the user clicks the search button, all the images matching the aforementioned searching criteria are retrieved and the user can now download the desired image products. As Fig. 5 shows, the system retrieves, in a table, a list of the image acquisitions together with their associated

Algorithm 2 Matching procedure used by the geolocation matching algorithm.

```
procedure POINTINSIDE(polygonPoints,testx,testy)
    NUMPOINTS = 4
    out = 0
    if testx < MIN(polygonP.x) OR testx > MAX(polygonP.x) OR testy < MIN(polygonP.y) OR testy > MAX
    (polygon.y) then
        j = NUMPOINTS-1
        for i = 0 to NUMPOINTS do
            z = polygonP[j].x - polygonP[i].x)* (testy - polygonP[i].y) / (polygonP[j].y - polygonP[i].y) +
            polygonP[i].x
            if (polygonP[i].y > testy =! polygonP.y[j] > testy) AND (testx < z) then
                c =! c
            end if
            j = i
        end for
    end if
    return out
end Procedure
Procedure ANYPOINTINPOLYGON(imagePoints,selectedPoints)
    NUMPOINTS = 4
    for i = 0 to NUMPOINTS-1 do
        point = imagePoints[i]
        if POINTINSIDE(selectedPoints,point.x,point.y) then
            return true
        end if
    end for
    for i = 0 to NUMPOINTS-1 do point = selectPoints[i]
        if POINTINSIDE(imagePoints,point.x,point.y) then
            return true
        end if
    end for
    return false
end procedure
Procedure PLANEINTERSECTION(imagePoints,selectedPoints)
    NUMPOINTS = 4
    j = NUMPOINTS – 1
    for i = 0 to NUMPOINTS-1 do
        if (Line(imagePoints[j],imagePoints[i]) ∩ Line(selectedPoints[0],selectedPoints[1])) OR
```

(*Line(imagePoints[j],imagePoints[i])* ∩ *Line(selectedPoints*[1],*selectedPoints*[2])) OR

(*Line(imagePoints[j],imagePoints[i])* ∩ *Line(selectedPoints*[2],*selectedPoints*[3])) OR

(*Line(imagePoints[j],imagePoints[i])* ∩ *Line(selectedPoints*[3],*selectedPoints*[0])) **then**

return true

else

j = i

end if

end for

return false

end procedure

products; this table is fully interactive and allows the user to browse among the image metadata and products. In the following subsection, we explain how the downloads (which can involve multiple users concurrently accessing the database) have been implemented in our geo-portal.

3.4 *Downloading*

The developed geo-portal has been designed to facilitate the access to the products which are required by users. Once the scenes of interest have been retrieved using the searching procedure described in the previous subsection, the user can select and download the products associated with the image matching the search criteria. In this regard, the geo-portal offers the capability to browse among the products of the images resulting from the filtering procedure and to individually select them for download. In addition, as Fig. 5 shows, the main panel of the browser includes a list of the available products which offer the capability to download the selected products of all the images selected in the table. A file storage server (based on the `FTP` protocol) is used for downloading purposes, so the server creates a folder with all the requested products that

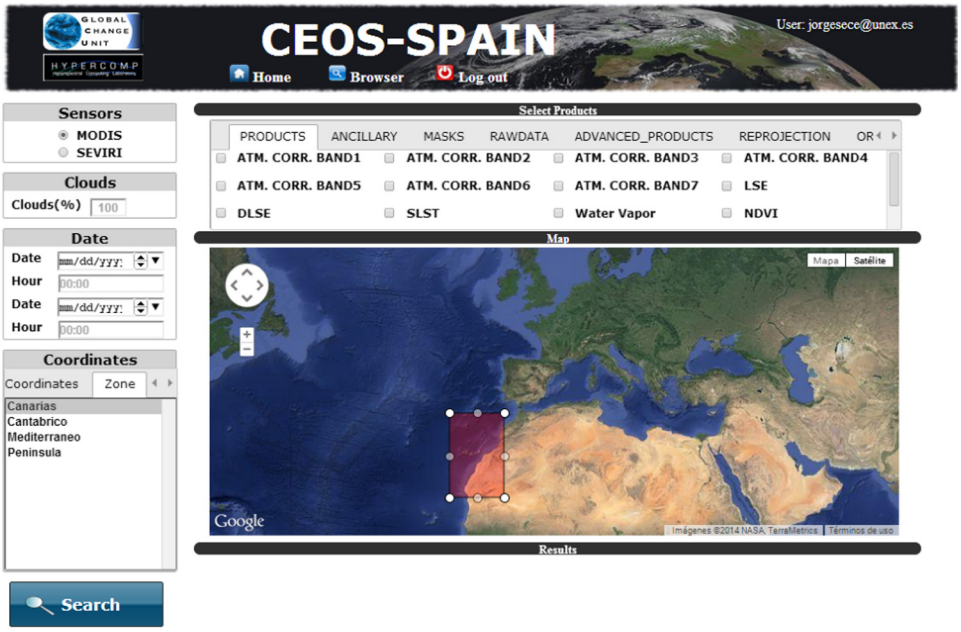

Fig. 4 Browser interface of the developed geo-portal.

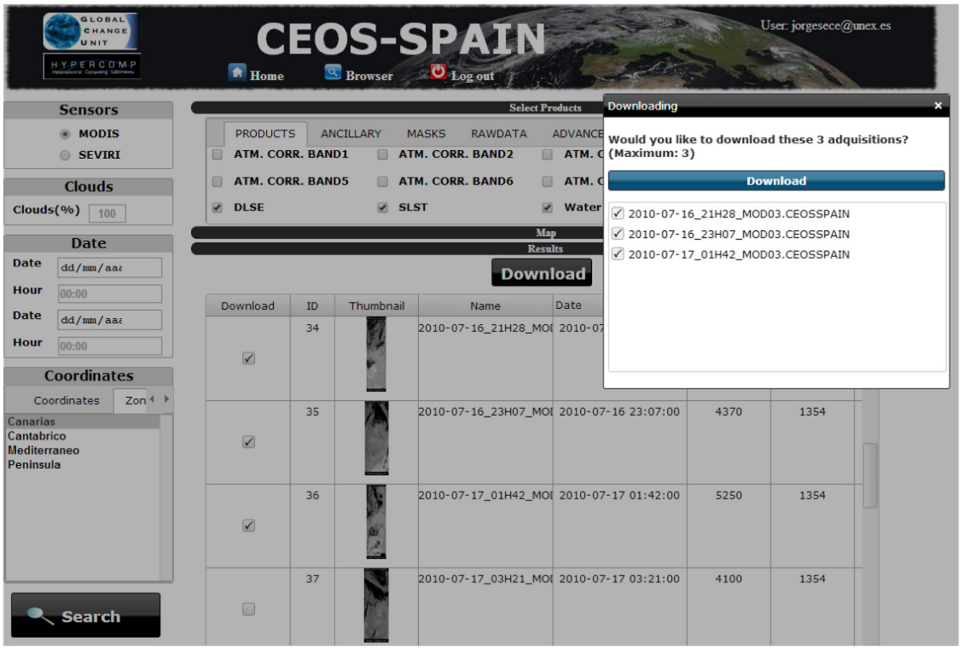

Fig. 5 Search results retrieved by the browser interface.

are available for the user to download. The selected products will be deleted from the server after a number of days (variable value). In this way, once the user executes the download option by clicking the corresponding button in the browser (see Fig. 5), the system creates the temporary folder, copies the selected products to the folder, and shows a pop-up message to the user together with the FTP download link. As mentioned before, the system has been implemented so as to support a large number of simultaneous connections and concurrent data downloads and is able to execute the queries with a high performance and with significant quality of service. In the following section, we provide an experimental evaluation of the system in terms of geolocation accuracy and computational efficiency in resolving the incoming queries.

4 Experimental Results

In this section, we evaluate the proposed geo-portal from two different perspectives: the efficiency in the retrieval of data products and the accuracy of the proposed geolocation matching algorithm. The section is organized as follows. In Sec. 4.1, we describe the MODIS/SEVIRI data sets and products used for our experimental validation. In Sec. 4.2, we illustrate the accuracy of the proposed geolocation matching algorithm used to retrieve products from our geo-portal. Finally, Sec. 4.3 performs an evaluation of the computational performance and response times measured in the retrieval process.

4.1 *Data and Products*

The experiments have been carried out using the full database of MODIS/SEVIRI images which have been processed (using the methodology described in Sec. 2) at UCG/IPL from July 2010 to January 2014 (in the case of MODIS) and from July 2007 to January 2012 (in the case of SEVIRI). This comprises a total of 7626 scenes and 165,406 products of MODIS (occupying a total space of more than 7 terabytes of products) and a total of 163,813 scenes and 313,345 products of SEVIRI (occupying a total space of more than 10 terabytes of products). For the MODIS data, it should be noted that the MODIS instrument provides images from (plus/minus) a 55 deg scanning pattern at the EOS orbit of 705 km, achieving a 2330-km swath. Thus, the features of these images are different in every acquisition. This includes width, height, or geolocation. In this way, two images from the same area can have different dimensions (width of

1354 ± 10 pixels and height of 5000 ± 200 pixels). This aspect complicated the geolocation process for these images, as indicated before. In order to illustrate this issue further, the following subsection provides an evaluation of the geolocation retrieval accuracy in the case of MODIS data.

4.2 *Geolocation Retrieval Accuracy*

The accuracy of the proposed geolocation-based retrieval system has been evaluated using a case study based on a query centered in the Canary Islands (35 deg north latitude, –9 deg south latitude, 20 deg east longitude, and –20 deg west longitude), as indicated in the user-drawn polygon depicted in Fig. 4. For illustrative purposes, the query was performed for a specific day (July 12, 2010), in which five different MODIS images were returned. For simplicity, we did not apply the cloudiness threshold in this experiment to remain focused on the evaluation of the geolocation results. For illustrative purposes, Fig. 6 graphically illustrates the geolocation accuracy achieved by our system in this particular experiment. More specifically, in Fig. 6, the red polygons represent a region of interest defined by the user (see Fig. 4), and the blue polygons represent the available MODIS images collected at different times on July 12, 2010. The intersection areas are displayed in cyan color. As shown by Fig. 6, three different images exhibited some degree of overlapping with the user-defined area. Note that the images acquired by MODIS at 01 h 24 min and 12 h 29 min did not overlap at all with the user-defined area; hence, these images were not retrieved by the geo-portal. In turn, the image acquired by MODIS at 03 h 02 min, 10 h 48 min, and 21 h 52 min exhibited some (partial) overlapping with the user-defined search area and were retrieved. We conducted several additional experiments using a larger number of involved images and user-defined searching areas with the same accuracy results, which confirmed the high precision of the geolocation matching algorithms developed for the geo-portal.

4.3 *Efficiency in Retrieval*

In this subsection, we evaluate the retrieval performance of the proposed geo-portal. For this purpose, we considered three different types of queries and measured the time in seconds from the query execution to the query completion, i.e., the effective time that the geo-portal took in order to provide the data solicited by the user for download purposes. Specifically, the types of queries considered in our tests were the following ones:

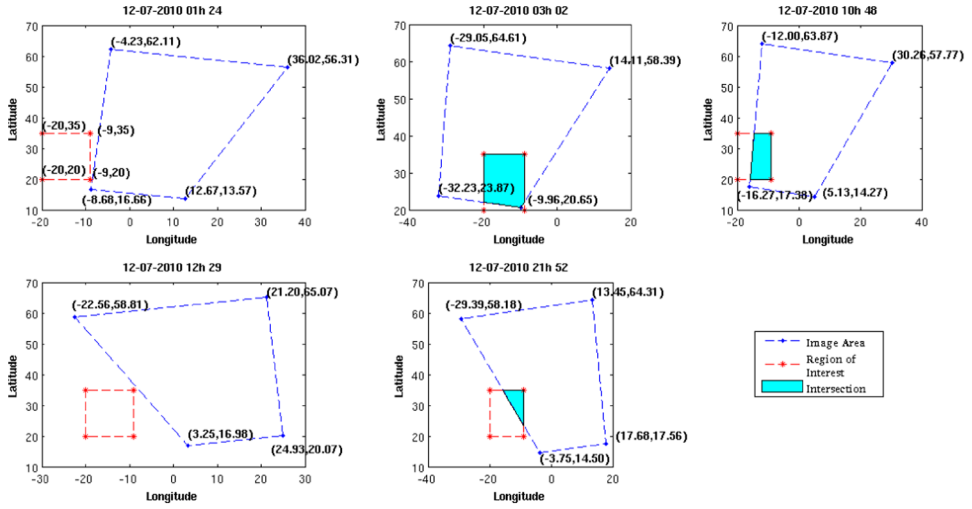

Fig. 6 A case study illustrating the geolocation matching accuracy of the developed geo-portal. The red polygons represent a region of interest defined by the user (centered over the Canary Islands, as depicted in Fig. 4) and the blue polygons represent the available moderate resolution imaging spectroradiometer (MODIS) images at different hours on July 12, 2010. The intersection areas are displayed in cyan color. In our experiment, only the cases in which there was overlap between the user-defined area and the available images resulted in data retrievals, which confirmed the good performance of the geolocation matching algorithm.

Table 3 Time (in seconds) that the geo-portal took to complete several types of queries applying different filters when exploring the whole database of MODIS/SEVIRI images. The images are filtered by date from July 2010 to January 2014 (in the case of MODIS) and from July 2007 to January 2012 (in the case of SEVIRI). In the queries based on a region of interest, we used an area centered over the Canary Islands depicted in Fig. 4. The cloudiness threshold considered in experiments was 80%, so that we filtered out the images containing more clouds than established in this threshold.

	Only date filter (SEVIRI images)	Only date filter (MODIS images)	Region of interest (MODIS images)	Cloudiness and region of interest (MODIS images)
Images retrieved	163,813	7626	5153	2592
Time (seconds)	0.008	0.008	9.101	37.078

- In the first type of query, we used a no filter scenario so that all the images from the same sensor could be retrieved. We performed this query for all the MODIS data and also for all the SEVIRI data, so that we could evaluate the performance of the system in retrieving all the data stored in the system by sensor type.
- In the second type of query, we analyzed the performance of the interest region filter. In this case, we used the same case study illustrated in the previous subsection, in which a query centered in the Canary Islands (35 deg north latitude, –9 deg south latitude, 20 deg east longitude, and –20 deg west longitude) was used after a user-defined region was established in the map panel of the geo-portal browser as depicted in Fig. 4.
- The third type of query analyzed the cloudiness threshold filter in combination with the interest region filter. This means that, for the considered user-defined region of interest centered in the Canary Islands and depicted in Fig. 4, we retained only those images that contain less than 80% cloudiness and discarded the rest. In all cases, we avoided establishing a filter for the retrieval of images based on the date in order to have a complete exploration of the whole database in multitemporal fashion.

As shown by Table 3, the retrieval times were quite fast for the three types of considered queries. The fastest cases correspond to the retrieval of all MODIS images and all SEVIRI images, which took less than 1 s to be completed. This is because the only filter applied in the query was the one given by the sensor type, which allowed for a very fast retrieval of the images corresponding to each type of sensor. In any event, given the very high number of images retrieved (7626 for MODIS and 163,813 for SEVIRI), we consider that the retrieval times were extremely fast. This indicates that the architecture of the proposed system can handle large volumes of data while providing very fast response times for the queries, implemented directly in the Mysql database manager. When the region of interest was defined, the query based on the considered region centered around the Canary Islands returned 5153 MODIS scenes, which is also a considerable amount of information. In this case, the geo-portal could provide the result of the query in approximately 9 s. Finally, the most complex query executed was completed in approximately 37 s. Such a response time is due to the fact that the cloudiness threshold was applied in a combined fashion with the region of interest filter, which means 30 combined comparisons for each image, since the cloudiness in the image is split into 30 quarters. Thus, this query is more complex in terms of execution than the previously considered ones. Still, the retrieval time in this case is considered to be quite appropriate bearing in mind that the query took as input the whole MODIS image database which comprises approximately 8 terabytes of data. At this point, we reiterate that the queries retrieve the images and also their products, but no product-related filters are available in the searching process since all the products of an image have the same query parameters.

5 Conclusions and Future Work

In this paper, an on-line geo-portal has been developed to manage a standardized data repository for multispectral images and their advanced products, which supports dissimilar sensors in order

to provide a wide perspective of the studied areas. A main characteristic of our geo-portal is that it provides access to processed final products. This eliminates the need to perform the processing of the data offline by integrating the data processing into the geo-portal. The data processing is accomplished in real time, i.e., as soon as the MODIS/SEVIRI data are collected by the receiving antenna our system obtains the resulting products and stores them in our database, which also handles the raw data. This makes the final product immediately available to the wide remote sensing community and allows for a detailed exploration of the high-level products obtained after the data processing.

The geo-portal has been designed in a modular way and implemented using advanced software and hardware infrastructures, allowing for the fast execution of queries embedded into our database engine as stored procedures. Most importantly, the geo-portal includes the possibility to perform geolocation-based product retrieval by defining regions of interest (and applying several types of filters) in a user-friendly browser that allows for a complete interaction with a map server such as Google Maps. Here, the map server is used to perform interactive-based queries on user-defined regions of interest. These regions are very easy to define and the user has the possibility of selecting an area and visualizing the overlapping products available in the system in a very intuitive manner, which enhances the usability of the system.

In terms of storage and retrieval capacity, the geo-portal currently provides impressive features: more than 9000 MODIS acquisitions and 200,000 resulting products (products occupy a total space of more than 11 terabytes of data) and more than 300,000 SEVIRI acquisitions and 600,000 resulting products (products occupy a total space of more than 17 terabytes of data). These products can be retrieved in a very fast manner and downloaded for further analyses. It should be noted that the amount of data available for download keeps growing as new acquisitions are processed and added to the database. This results in a massive amount of information that is now fully available to the remote sensing community through the developed geo-portal. As future work, we plan to include images and products collected from other sensors in addition to additional MODIS/SEVIRI products. We are also planning on integrating additional content-based image retrieval functionalities into the geo-portal, in the vein of the developments recently presented in Ref. 66.

Acknowledgments

This work has been supported by the Calibration of Earth Observation Satellites in Spain (CEOS-SPAIN) project funded by the Spanish Ministry of Science and Innovation (AYA2011-29334-C02).

References

1. X.-X. Xiong et al., "Overview of NASA Earth observing systems Terra and Aqua moderate resolution imaging spectroradiometer instrument calibration algorithms and on-orbit performance," *J. Appl. Remote Sens.* **3**(1), 032501 (2009).
2. G. Toller et al., "Status of earth observing system Terra and Aqua moderate-resolution imaging spectroradiometer level 1B algorithm," *J. Appl. Remote Sens.* **2**(1), 023505 (2008).
3. B.-C. Gao, R.-R. Li, and X.-X. Xiong, "Possible enhancement to specifications of several moderate resolution imaging spectroradiometer visible and near-IR channels for improved earth observations," *J. Appl. Remote Sens.* **1**(1), 013504 (2007).
4. L. Wang et al., "Impact assessment of Aqua MODIS band-to-band misregistration on snow index," *J. Appl. Remote Sens.* **1**(1), 013531 (2007).
5. F. Pasternak, P. Hollier, and J. Jouan, "SEVIRI, the new imager for Meteosat Second Generation," in *Proc. IEEE Int. Geoscience and Remote Sensing Symp. (IGARSS)*, pp. 1094–1099, IEEE Press, Piscataway, New Jersey (1993).
6. X. Xiong, N. Che, and W. Barnes, "Terra MODIS on-orbit spatial characterization and performance," *IEEE Trans. Geosci. Remote Sens.* **43**, 355–365 (2005).
7. S. Platnick et al., "The MODIS cloud products: algorithms and examples from Terra," *IEEE Trans. Geosci. Remote Sens.* **41**, 459–473 (2003).

8. H. Shen, C. Zeng, and L. Zhang, "Recovering reflectance of AQUA MODIS band 6 based on within-class local fitting," *IEEE J. Sel. Topics Appl. Earth Observ. Remote Sens.* **4**, 185–192 (2011).
9. J.-C. Jiménez-Muñoz et al., "Temperature and emissivity separation from MSG/SEVIRI data," *IEEE Trans. Geosci. Remote Sens.* **52**(9), 5937–5951 (2014).
10. M. Romaguera, J. A. Sobrino, and F. S. Olesen, "Estimation of sea surface temperature from SEVIRI data: algorithm testing and comparison with AVHRR products," *Int. J. Remote Sens.* **27**(22), 5081–5086 (2006).
11. M. Atitar and J. A. Sobrino, "A split-window algorithm for estimating LST from Meteosat 9 data: test and comparison with in situ data and MODIS LSTs," *IEEE Geosci. Remote Sens. Lett.* **6**, 122–126 (2009).
12. J. A. Sobrino, J. El Kharraz, and Z.-L. Li, "Surface temperature and water vapour retrieval from MODIS data," *Int. J. Remote Sens.* **24**(24), 5161–5182 (2003).
13. J. A. Sobrino and Y. Julien, "Trend analysis of global MODIS-Terra vegetation indices and land surface temperature between 2000 and 2011," *IEEE J. Sel. Topics Appl. Earth Observ. Remote Sens.* **6**, 2139–2145 (2013).
14. J. A. Sobrino and M. Romaguera, "Water vapour retrieval from Meteosat 8/SEVIRI observations," *Int. J. Remote Sens.* **29**(3), 741–754 (2008).
15. C. J. Tucker, "Red and photographic infrared linear combinations for monitoring vegetation," *Remote Sens. Environ.* **8**(2), 127–150 (1979).
16. G. Gutman and A. Ignatov, "The derivation of the green vegetation fraction from NOAA/AVHRR data for use in numerical weather prediction models," *Int. J. Remote Sens.* **19**(8), 1533–1543 (1998).
17. F. Camacho de Coca et al., "Prototyping of cover product over Africa based on existing CYCLOPES and JRC products for VGT4Africa," in *Proc. 2nd Workshop on Recent Advances in Quantitative Remote Sensing (RAQRS)*, Valencia, Spain, Vol. 1, pp. 722–727 (2006).
18. B. Tan et al., "An enhanced TIMESAT algorithm for estimating vegetation phenology metrics from MODIS data," *IEEE J. Sel. Topics Appl. Earth Observ. Remote Sens.* **4**, 361–371 (2011).
19. L. Lei, Z. Zeng, and B. Zhang, "Method for detecting snow lines from MODIS data and assessment of changes in the Nianqingtanglha mountains of the Tibet plateau," *IEEE J. Sel. Topics Appl. Earth Observ. Remote Sens.* **5**, 769–776 (2012).
20. T.-Y. Chang et al., "Estimation of root zone soil moisture using apparent thermal inertia with MODIS imagery over a tropical catchment in northern Thailand," *IEEE J. Sel. Topics Appl. Earth Observ. Remote Sens.* **5**, 752–761 (2012).
21. J. Knight and M. Voth, "Mapping impervious cover using multi-temporal MODIS NDVI data," *IEEE J. Sel. Topics Appl. Earth Observ. Remote Sens.* **4**, 303–309 (2011).
22. N. Torbick et al., "Monitoring rice agriculture in the Sacramento Valley, USA, with multitemporal PALSAR and MODIS imagery," *IEEE J. Sel. Topics Appl. Earth Observ. Remote Sens.* **4**, 451–457 (2011).
23. F. Tian et al., "Studies on the relationships between land surface temperature and environmental factors in an inland river catchment based on geographically weighted regression and MODIS data," *IEEE J. Sel. Topics Appl. Earth Observ. Remote Sens.* **5**, 687–698 (2012).
24. D. Sun, Y. Yu, and M. D. Goldberg, "Deriving water fraction and flood maps from MODIS images using a decision tree approach," *IEEE J. Sel. Topics Appl. Earth Observ. Remote Sens.* **4**, 814–825 (2011).
25. A. S. Ardakani et al., "Spatial and temporal analysis of fires detected by MODIS data in northern Iran from 2001 to 2008," *IEEE J. Sel. Topics Appl. Earth Observ. Remote Sens.* **4**, 216–225 (2011).
26. B. Geiger et al., "Land surface albedo derived on a daily basis from Meteosat Second Generation observations," *IEEE Trans. Geosci. Remote Sens.* **46**, 3841–3856 (2008).
27. M. O. Rasmussen et al., "Directional effects on land surface temperature estimation from Meteosat second generation for Savanna landscapes," *IEEE Trans. Geosci. Remote Sens.* **49**, 4458–4468 (2011).
28. B. Hirn, C. Di Bartola, and F. Ferrucci, "Combined use of SEVIRI and MODIS for detecting, measuring, and monitoring active lava flows at erupting volcanoes," *IEEE Trans. Geosci. Remote Sens.* **47**, 2923–2930 (2009).

29. J. A. Sobrino, Y. Julien, and G. Soria, "Phenology estimation from Meteosat Second Generation data," *IEEE J. Sel. Topics Appl. Earth Observ. Remote Sens.* **6**, 1653–1659 (2013).
30. N. Jaiswal and C. M. Kishtawal, "Objective detection of center of tropical cyclone in remotely sensed infrared images," *IEEE J. Sel. Topics Appl. Earth Observ. Remote Sens.* **6**, 1031–1035 (2013).
31. R. M. A. Timmermans et al., "The added value of a proposed satellite imager for ground level particulate matter analyses and forecasts," *IEEE J. Sel. Topics Appl. Earth Observ. Remote Sens.* **2**, 271–283 (2009).
32. S. Liang et al., "Review on estimation of land surface radiation and energy budgets from ground measurement, remote sensing and model simulations," *IEEE J. Sel. Topics Appl. Earth Observ. Remote Sens.* **3**, 225–240 (2010).
33. LAADS, "Level 1 and atmosphere archive and distribution system," http://ladsweb.nascom.nasa.gov/ (accessed 7 June 2014).
34. EarthExplorer, "USGS EarthExplorer," http://earthexplorer.usgs.gov (accessed 7 June 2014).
35. M. 2.0, "USGS MRT Wev 2.0," https://mrtweb.cr.usgs.gov/ (accessed 7 June 2014).
36. Glovis, "USGS global visualization viewer," http://glovis.usgs.gov/ (accessed 7 June 2014).
37. MRT, "MODIS reprojection tool (MRT)," https://lpdaac.usgs.gov/tools/modisreprojectiontool (accessed 7 June 2014).
38. GCU/IPL, "Global Change Unit, Image Processing Laboratory at University of Valencia," http://www.uv.es/ucg (January 2015).
39. https://www.google.com/maps (January 2015).
40. http://ceosspain.lpi.uv.es (January 2015).
41. http://www.exelisvis.com/ProductsServices/IDL.aspx (January 2015).
42. H. Rahman and G. Dedieu, "SMAC: a simplified method for the atmospheric correction of satellite measurements in the solar spectrum," *Int. J. Remote Sens.* **15**(1), 123–143 (1994).
43. http://eostation.scanex.ru/software.html (January 2015).
44. F.-N. Kogan, "NOAA plays leadership role in developing satellite technology for drought watch," *Earth Observ. Mag.*, 18–21 (1994).
45. W. Lucht et al., "A comparison of satellite-derived spectral albedos to ground-based broadband albedo measurements modeled to satellite spatial scale for a semidesert landscape," *Remote Sens. Environ.* **74**, 85–98 (2000).
46. J. El Kharraz, "Determinación de la temperatura de la superficie terrestre a partir de datos MODIS," PhD Thesis, Univ. of Valencia (2009)
47. Y. Julien et al., "Near real-time estimation of water vapor column from MSG SEVIRI thermal infrared bands: implications for land surface temperature retrieval," *IEEE Trans. Geosci. Remote Sens.* submitted.
48. http://symfony.com.
49. http://www.json.org.
50. http://www.w3.org/TR/html51.
51. http://www.w3.org/Style/CSS.
52. http://jquery.com.
53. http://www.w3.org/Protocols/.
54. http://www.mysql.com.
55. http://www.w3.org/Protocols/rfc959/.
56. http://www.dell.com/us/business/p/network-file-storage.
57. http://www.dellstorage.com/WorkArea/DownloadAsset.aspx?id=2966.
58. http://www.dell.com/learn/us/en/04/campaigns/dell-hard-drives.
59. http://ark.intel.com/products/64588/intel-xeon-processor-e5.
60. http://www.dell.com/downloads/global/products/pvaul/en/perc-technical-guidebook.pdf.
61. http://www.dell.com/us/business/p/powervault-md1200/pd.
62. http://www.dell.com/downloads/global/products/pvaul/en/perc-technical-guidebook.pdf.
63. http://www.samba.org/samba/docs/man/Samba4-HOWTO/protocol.html (January 2015).
64. IMAPP, "International MODIS/AIRS processing package," http://eostation.scanex.ru/software.html (27 May 2014).

65. M. Shimrat, "Algorithm 112: position of point relative to polygon," *Commun. ACM* **5**(8), 434 (1962).
66. J. Sevilla and A. Plaza, "A new digital repository for hyperspectral imagery with unmixing-based retrieval functionality," *IEEE J. Sel. Topics Appl. Earth Observ. Remote Sens.* **7**(6), 2267–2280 (2014).

Jorge Sevilla received his BS and MS degrees in computer sciences from the University of Extremadura in 2006 and 2008, respectively, where he is currently pursuing his PhD degree. He has been a research intern with the National Institute of Nuclear Physics, Catania, Italy. He has also been a visiting researcher with the West University of Timisoara, Romania. His research interests include hyperspectral image analysis, efficient implementations, development of digital repositories, and content-based image retrieval. He has served as reviewer for several journals and conferences. He is a member of the Hyperspectral Computing Laboratory (HyperComp).

Yves Julien is a researcher at the Global Change Unit (http://www.uv.es/ucg) at the University of Valencia, Spain. He obtained his PhD degree in Earth physics and thermodynamics from the University of Valencia (Spain) and in electronics, electrotechnics, and automatics (specialized in remote sensing) from the University of Strasbourg, France, in 2008. He is the author of more than 22 international papers (http://www.uv.es/juy/publications.htm). His research interests include temperature and vegetation indices interactions, as well as time series analysis for land cover dynamic monitoring.

Guillem Sória received his PhD degree in Earth physics and thermodynamics from the University of Valencia, Spain, in 2006. He is the author of more than 20 international papers. Currently, he is a research scientist with the Global Change Unit (http://www.uv.es/ucg) at the University of Valencia. His research interests include thermal remote sensing and the design and implementation of experimental field campaigns related to thermal parameters retrieval.

José A. Sobrino is a professor of physics and remote sensing and head of the Global Change Unit (http://www.uv.es/ucg) at the University of Valencia, Spain. He is the author of more than 100 papers and the coordinator of the European projects WATERMED and EAGLE. He has been a member of ESAC (Earth Science Advisory Committee) of ESA (European Space Agency) since November 2003. He was the chairperson of First, Second, and Third International Symposium RAQRS (Recent Advances in Quantitative Remote Sensing) http://www.uv.es/raqrs. His research interests include atmospheric correction in visible and infrared domains, the retrieval of emissivity and surface temperature from satellite images, and the development of remote sensing methods for land cover dynamic monitoring.

Antonio Plaza is an associate professor (with accreditation for full time professor) with the Department of Technology of Computers and Communications, University of Extremadura, where he is the head of the Hyperspectral Computing Laboratory (HyperComp). He authored more than 400 publications, including 136 JCR journal papers (81 in IEEE journals), 20 book chapters, and over 240 peer-reviewed conference proceeding papers (94 in IEEE conferences). He is a recipient of the recognition of best reviewers of the *IEEE Geoscience and Remote Sensing Letters* (in 2009) and a recipient of the recognition of best reviewers of the *IEEE Transactions on Geoscience and Remote Sensing* (in 2010), a journal for which he served as associate editor from 2007 to 2012. Currently, he is serving as the editor-in-chief of the *IEEE Transactions on Geoscience and Remote Sensing* journal (since January 2013). Additional information: http://www.umbc.edu/rssipl/people/aplaza.